TECHNICAL ARTICLE

Development of Cost-Effective Microstructure and Isothermal Oxidation-Resistant Bond Coats on Inconel 718 by Atmospheric Plasma-Sprayed NiCoCrAlFe High-Entropy Alloy

KASHIF MEHMOOD [iD],[1,4] MUHAMMAD IMRAN,[2] LIAQAT ALI,[2] MALIK ADEEL UMER,[1,5] MUSHARAF ABBAS,[3] and MOHSIN SALEEM[1]

1.—School of Chemical and Materials Engineering (SCME), National University of Science and Technology, Islamabad, Pakistan. 2.—Department of Chemistry, Government College University, Lahore, Pakistan. 3.—School of Materials Science and Engineering, University of New South Wales, Sydney, NSW 2052, Australia. 4.—e-mail: chkashif94@gmail.com. 5.—e-mail: umer.adeel@scme.nust.edu.pk

Ni-based superalloy (Inconel 718) has been widely employed in aircraft, gas turbine engines, and turbocharger rotor equipment, due to its high strength and long fatigue life, but inadequate oxidation resistance has restricted high-temperature applications. In the current study, a NiCoCrAlFe high-entropy alloy (HEA) coating was fabricated on Inconel 718 using low energy ball-milled/blended elemental powders thermally sprayed by an atmospheric plasma spraying process. The microstructural and isothermal oxidation behavior of the NiCoCrAlFe HEA bond coats at 1000°C was studied. The result revealed that the microstructure of the HEA coatings consists of dark and light phases in the lamellar structure. The dark phases are relatively hard and are oxides, while the soft phase is the HEA phases spread in the microstructure. The novel NiCoCrAlFe high-entropy bond coat exhibits a considerably low oxidation rate and slow (Al_2O_3) TGO formation on the surface of the bond coats at elevated temperatures and exposure for extended durations. In conclusion, the present study provides a workable approach for enhancing the oxidation resistance of Inconel 718 alloy in high-temperature conditions.

INTRODUCTION

In recent years, High Entropy Alloys (HEAs) have emerged as a potential candidate for various structural applications,[1] first presented by Yeh et al. in 1996 and then reported in their publication in 2004.[2] Cantor et al. designated them 'multi-component alloys' in the same year.[3] HEAs are constituted of the equimolar ratio of more than four principal alloying elements, and consequently improved features have been obtained, like[4] mechanical strength,[5,6] extra-ordinary oxidation,[7] corrosion resistance,[8] high resistivity, magnetic properties, and high-temperature performance.[9] These properties can be tailor-made by fluctuating and changing the compositions of the constituting elements making them even more captivating materials.[8] Recently, HEAs have been employed as bond coating or surface coating prepared by laser coating.[10] High-velocity oxygen fuel coating is a commonly used coating technique,[11] because it provides a high powder velocity and a comparatively lower spraying temperature,[12–14] In addition, selective laser melting, is a 3-D printing, prototype, or additive manufacturing technique,[16] but it requires an inert gas supply.[15,16] Furthermore, there are the electrospark deposition technique,[17] cold spraying, but with the loss of ductility of the coating because of plastic deformation process,[18] low-pressure plasma spraying and flame spraying, which have the major disadvantages of high porosity and oxides, and a low density of metal deposits,[8,19,20] and laser

cladding[21,22] but all these methods have shortcomings in terms of significant upfront cost, low deposition rates, and requiring high-energy fuel.

Atmospheric plasma spraying (APS)[20,23,24] has appeared as a promising technique to deposit different feedstock materials as well as HEAs on different substrates. In this technique, the feedstock to be deposited is generally in the form of powder or in some cases wire. A DC arc is struck (normally using on the order of 30 V and 300–800 A) within the anode and cathode to generate plasma in the carrier gas, which is usually a mixture of argon (Ar) plus hydrogen (H$_2$) or helium (He) and nitrogen (N$_2$).[25] The plasma jet temperature is on the order of c. 16,000 K. The feedstock is heated and projected onto a substrate.[26] Molten or semi-molten drops quickly solidify, flatten, and form deposits on the substrate in the form of a coating. Generally, the solidified feedstock stays adherent to the substrate as a coating by mechanical locking.[27] Recently, the isothermal oxidation performance of various HEAs, like (FeCoNiMo)90(Al/Cr)10, has been studied by Chen et al., along with the mechanical properties.[28] Similar oxidation behavior of CoCrNi, CoCrNiMn, and CoCrNiMnFe equimolar alloys has also been reported.[29,30] Thus, in addition to being a potential candidate for structural and functional materials, AlCoCrFeNi HEAs can also be applied as a surface coating or bond coat[31] for protection against high-temperature environments and to increase the robustness of the structural material.

In recent times, Ni-based superalloys have been gaining the attention of researchers owing to their extraordinary mechanical features, including tensile strength ($\sim$ 690 MPa), fatigue strength, stable microstructure, excellent physical characteristics, and holding strength at high temperatures ($\sim$ 800–1050°C.[32] These features make Ni-based superalloys suitable candidates for gas turbine engines, aircraft, and aero-turbine components. It has been reported that Ni-based superalloys are vulnerable to high-temperature oxidation. Hence, reasonable thermal barrier coatings (TBCs) are required to protect them against high-temperature oxidation. A multi-component alloy layer between the superalloy and the TBC is required to ensure better adherence.[33] In the current study, low-energy ball-milled/blended elemental powders were thermally sprayed by APS on Inconel 718 alloy. Various modern techniques have been employed to investigate the microstructural characterization and oxidation behavior at high temperatures of HEA coatings. Various parameters, including phases, the morphology of cross-sections, and elemental composition, were also investigated after oxidation.

EXPERIMENTAL

A WiseMix BML-2 (PMR-Labortechnik, Germany) 2-roll mill apparatus was used to prepare the HEA (NiCoCrAlFe) using > 99.5% pure corresponding elemental powders via low-energy ball-milling. Steel balls and polypropylene vials were used as the milling media with a powder to ball ratio of 1:10 and milling duration of 14 h. A STOE Panalytical XRD apparatus (Cu-K$_\alpha$ radiation, 0.02° step size, and duration of 20 s) was employed to examine the various phases that appeared after plasma spraying, annealing, and isothermal oxidation. SEM–EDS was employed to evaluate different parameters, including phases, microstructures, and the distribution of the elements (via point EDS analysis).

MATERIALS AND METHODS

Chemicals

Feedstock powder of elements Al, Co, Cr, Fe, and Ni ($\sim$ 99.5% purity) were procured from Greenearth Chem, Shanghai, China. To obtain a homogeneous mixture of the feedstock elements, ball-milling/blending was used before the experiment.

Ball Milling (Blending/Mixing) of Elemental Powders

All the elemental powders were mixed in equiatomic ratios in a polypropylene vial using a glove box apparatus to avoid contamination of the powders by air. Stainless steel balls having Ø10 were used and Ar was purged in the vial to maintain an inert atmosphere during the ball milling. The speed of the ball mill apparatus was 140 rpm and the ball to powder weight ratio (mass ratio) was 10:1. Mixing/blending of the equi-atomic powders was carried out for 14 h in a 2-roll ball-milling apparatus.[30]

Sample Preparation and Pre-heating of Substrates and Powder

Inconel 718 (2.54 × 2.54 cm) substrates were used for coating. The nominal chemical composition of the Ni-based super alloy (Inconel 718) used as the substrate is given in Table I. Cleaning was performed to remove any dust, oil, grease, or any foreign particles present on the surface. Surface activation was performed by using different techniques, like sand-blasting and grit-blasting, as they enhance the surface roughness which in turn results in better adhesion of the coating to the substrate. Other modern techniques for surface activation include laser ablation and water jet treatment. In the current study, we used grit-blasting to prepare our substrates for thermal spraying, and afterwards cleaned them by dipping them in acetone (CH$_3$COCH$_3$) to eradicate dirt and any impurities. To escalate the surface roughness of the substrates, a pressure of 0.40 MPa was used followed by air drying. Alumina (Al$_2$O$_3$) particles of 40–60 μm were grit-blasted on the substrates for surface preparation. Blended HEA powder as well as the substrates were pre-heated to remove any

Development of Cost-Effective Microstructure and Isothermal Oxidation-Resistant Bond Coats
on Inconel 718 by Atmospheric Plasma-Sprayed NiCoCrAlFe High-Entropy Alloy

241

Table I. Nominal composition of Inconel 718 Ni-based superalloy

Ni	Cr	Nb	Ti	Mo	Al	Co	Fe
Chemical composition in mass%							
53.53	18.45	5.31	0.95	3.02	0.48	0.27	Balance

Cu	Mn	C	Ta	P	B	S	Si
0.04	0.06	0.03	0.005	0.007	0.004	0.002	0.09

moisture present. The blended HEA powder was retained in the oven for 2 h at 25–150°C. The HEA powder was placed in a bowl and covered by an aluminum sheet to avoid any vaporization towards the oven wall. The pre-heating of the substrates was carried out by the flame of a spray gun giving several runs before turning on the powder feeder.[30]

Atmospheric Plasma Spraying of Bond Coatings onto the Substrates

An APS system (Metco 9MC; Sulzer Metco, New York, USA) was employed to coat the HEA on the surface of the superalloy with a stand-off distance of 250 nm.[30] To rapidly increase the temperature of the plasma jet, a primary operating gas (Ar) and a secondary gas (H_2) were used. A separate Ar gas source was used to convey the feedstock of the elemental powder (ball-milled) at a right angle (90°) to spawn the plasma jet. A robotic arm (YR-SK 16-J00 Motoman; Yaskawa Electric, Japan) was used to traverse across the substrate holders, and subsequently a plasma torch assembly was mounted on this arm.[30] The plasma-spraying operation parameters used are listed in Table II.

Controlled Atmosphere Heat Treatment (Annealing) of Bond Coats

After the APS of the bond coats, the post-heat treatment (annealing) was carried out in a tube furnace (Protherm PZF 12/50/700) for 4 h at 900°C in an inert atmosphere containing Ar (P (Ar) $\geq 1 \times 10^5$ Pa, $P(O_2) < 0.001$ Pa) for elemental diffusion and homogenization of the APS coatings.[30] These conditions were employed to provide the Ar gas with high purity and relatively high pressure compared with standard atmospheric pressure in order to limit the inflow of oxygen into the furnace. Consequently, minimizing the oxygen content results in preventing oxidation of the bond coats during this process.

Isothermal Oxidation Testing of the Bond Coats

A muffle furnace was employed to perform isothermal oxidation (ITO) testing of all the samples at 1000°C with exposure times of 5 h, 15 h, 50 h, and 100 h). The furnace was equipped with a temperature controller to retain the requisite temperature within ± 5°C. Briefly, the plasma-sprayed and annealed coatings of the HEA on the superalloy were exposed to the ITO atmosphere by placing in an alumina crucible with a heating rate of 30°C/min. The coating was removed after the exposure times of 5 h, 15 h, 50 h, and 100 h, followed by cooling in air for 45 min until the ambient temperature was reached. The samples obtained after ITO were examined via SEM to determine the morphology and phase transformation, while EDS was used to determine the elemental composition of a cross-section of the samples before and after ITO testing.

RESULTS AND DISCUSSION

Microstructural Studies

Microstructure and cross-section analysis of all the bond coats in the as-sprayed condition were performed by using a Leo Gemini Analytical SEM (ZEISS, Oberkochen, Germany), the annealed conditions were examined on a VEGA 3 TESCAN SEM, and, after isothermal oxidation, tested using a MAIA3 TESCAN SEM by varying the magnification. SEM micrographs of the bond coats in cross-section in the as-sprayed condition are shown in Fig. 1.

It is evident from viewing the SEM micrographs that the coating exhibits a splat morphology consisting of dark and light phases. Due to the high temperature of the plasma torch, the maximum powdered particles[30] which experienced the flame energy were fully melted, resulting in the forming of a splats morphology, while some of them which experienced a lower temperature adhered to the substrate in a partially molten state, as reported earlier by Ang et al.[34] is the coating was homogeneous and well-adhered to the superalloy substrate, with an average thickness of 150–180 μm. Overall, the coating deposition efficiency was good and a dense coating was attained. After the development of the APS bond coats, annealing was carried out for 4 h at 900°C in an inert atmosphere containing Ar a tube furnace (Protherm PZF 12/50/700).[30] After the heat treatment, microstructural studies were

Table II. Parameters for plasmaspraying operation

Parameters	Values	Parameters	Values
Arc voltage	70 (V)	Arc current	650 (A)
Rate of feeding powder	38 (g/min)	Feed gas flow	8 (Ar/slpm)
Gas flow (primary)	40 Ar/slpm)	Gas flow (secondary)	3.5 (H_2/slpm)
Stand-off distance	200 (mm)	Speed of torch (traverse)	190 (mm/s)
Type of nozzle	9 MB	Controller	9 MC

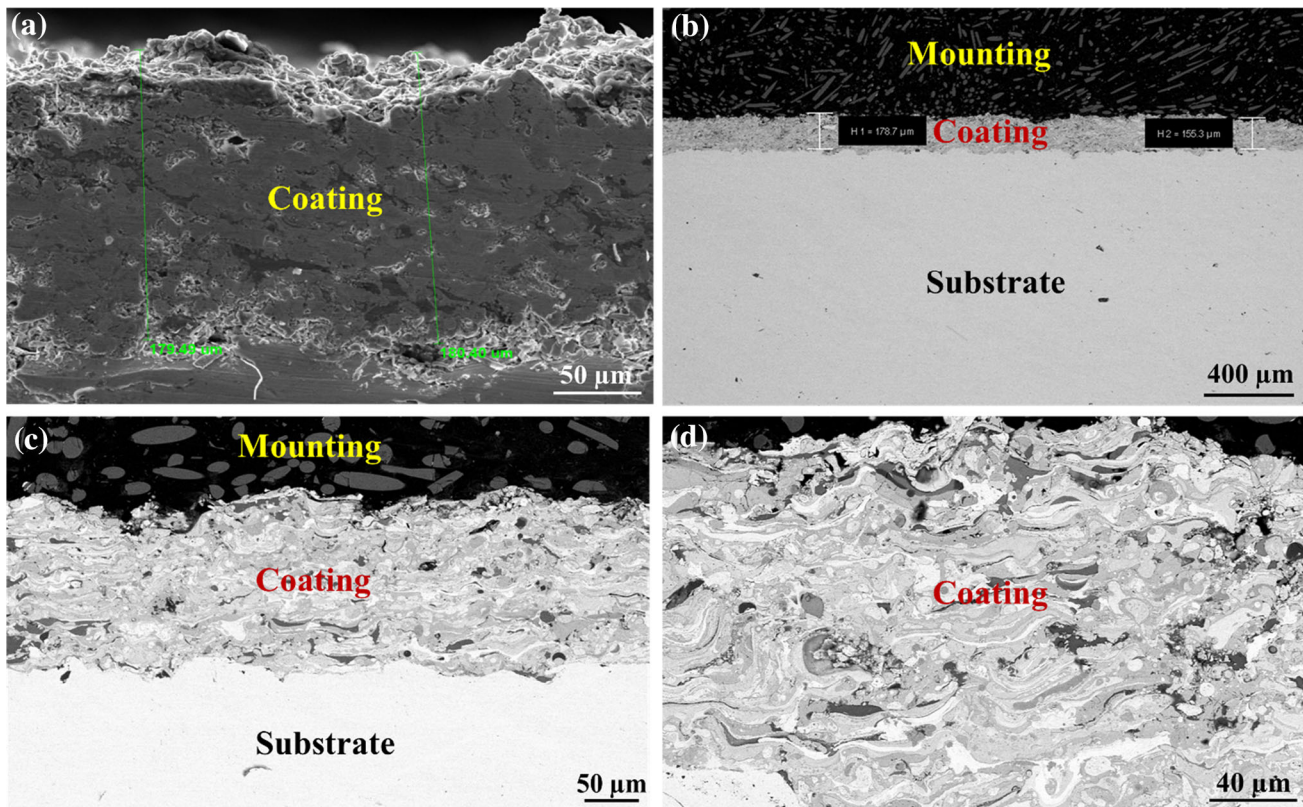The angle for the experiment was 90°.

Fig. 1. Cross-section microstructure of bond coats in as-sprayed condition: (a) SE mode, (b), (c), and (d) BSE mode.

carried out in cross-sections using a VEGA3 TES-CAN SEM.[30] The microstructure of the heat-treated (annealed) coatings revealed a lamellar structure just like it was in its as-coated form, but there was a major change perceived after annealing, such as the maximum formation of HEA phase fractions as compared to the other phases present in the bond coat.[30] Three types of phases were detected based on color contrast, i.e., dark gray phase, light gray phase, and white phase as reported earlier by Meghwal et al.[30,35] The coating morphology showed some pores, interlamellar micro-cracks, oxide stringers, voids, and a lamellar structure, as presented in Fig. 2.

The dark gray phases were hard and mainly consisted of spinels, and other oxides which solidified after plasma spraying, while the white phase is a soft phase compared to the light and dark gray phases, and is the solid solution which is the HEA.[35] As we annealed the samples in an inert atmosphere, it can be understood that the white phase fraction (HEA phase) is amplified, which is evident from the SEM images of the annealed samples, and proof of HEA development after post-heat treatment (annealing) of the plasma-sprayed bond coats, as shown in Fig. 3. Alongside the HEA fraction, some oxide stringers were found dispersed in the microstructure, which appeared as light and dark gray phases, by virtue of the high temperature of the plasma
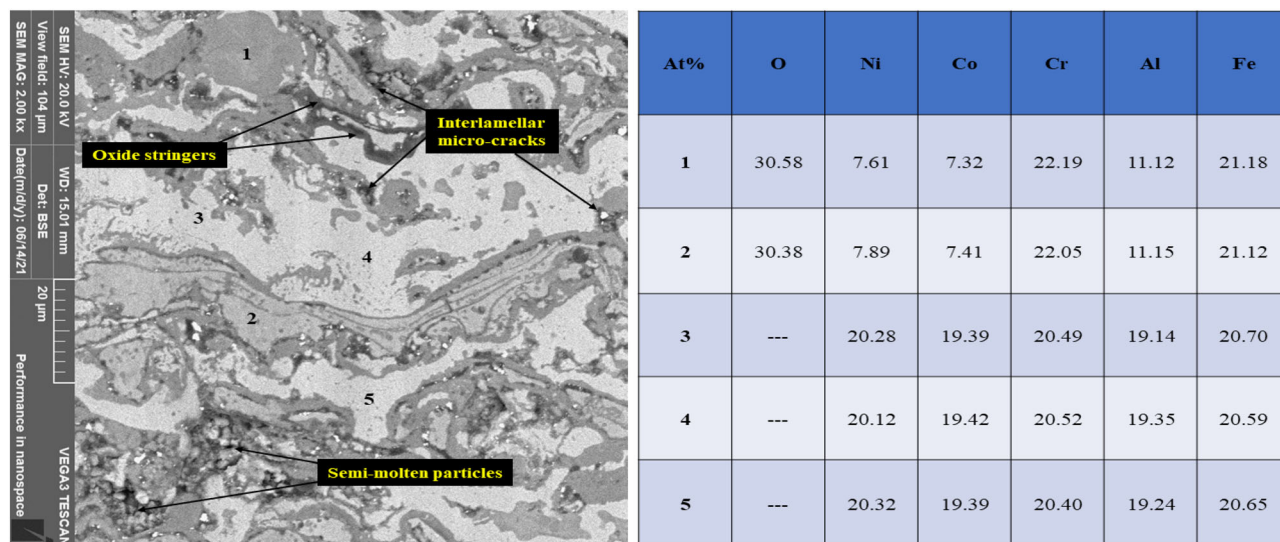
At%	O	Ni	Co	Cr	Al	Fe
1	30.58	7.61	7.32	22.19	11.12	21.18
2	30.38	7.89	7.41	22.05	11.15	21.12
3	---	20.28	19.39	20.49	19.14	20.70
4	---	20.12	19.42	20.52	19.35	20.59
5	---	20.32	19.39	20.40	19.24	20.65

Fig. 2. BSE (SEM) micrograph of annealed bond coat (left) and EDS at different points (right).
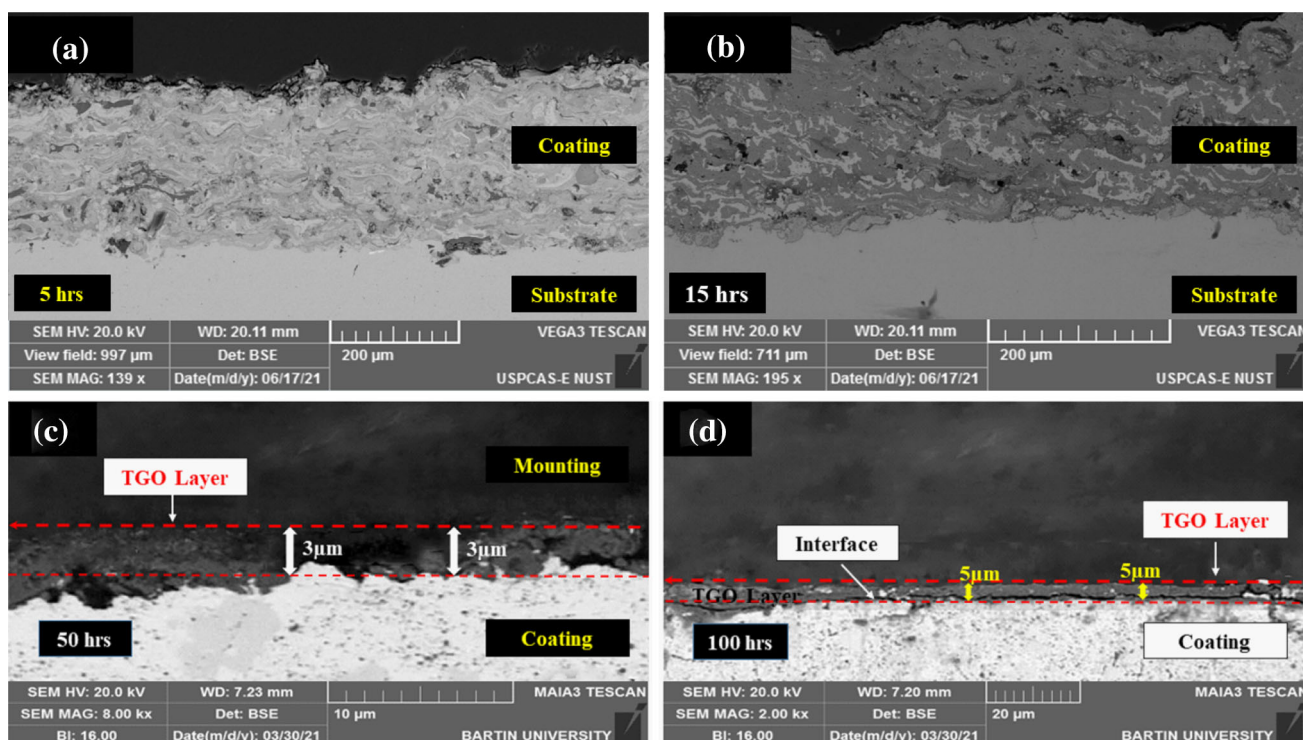
Fig. 3. SEM images after isothermal oxidation testing of coatings for: (a) 5 h, (b) 15 h, (c) 50 h, and (d) 100 h.

flame, due to which these oxides are formed and are a part of the sprayed coating, as seen in the microstructure of the annealed coatings. The annealing at 900°C for the specified time was enough for the diffusion of atoms into each other to form the HEA, which was not achieved completely prior to a later stage. The presence of Ar gas stopped any oxide formation while carrying out post-heat treatment (annealing), and facilitated the diffusion of elements for the formation of the alloy phase, which can be seen in the SEM images.[30]

ITO behavior of the prepared coatings was investigated in a Nabetherm muffle furnace to evaluate the thermal stability and to check the TGO formation on the bond coats for different exposure times. The samples were kept in the furnace at 1000°C for different times, i.e., 5, 15, 50, and 100 h, and were examined by BSE SEM after proper grinding and polishing of the cross-sections of the coatings. It was

found that, for the exposure of 5 h in oxidation testing, there is no significant change from its annealed state. However, some phases were a little altered, as shown in the microstructure depicting the formation of the spinel, chromia, and HEA phases after 15 h of oxidation testing.[36] No continuous TGO growth was observed even after 5 h and 15 h of oxidation testing. ITO testing of the bond coats for 50 h revealed the formation of the TGO layer, consisting of α-Al_2O_3, chromia (Cr_2O_3), and a small amount of spinel (AB_2O_4) structures, having an average thickness of 3 ± 0.50 μm, as shown in Fig. 3c. It displays poor adherence to the oxide scale owing to rutted growth of the TGO upon exposure to oxidation. Bond coats which were exposed to ITO for 100 h resulted in the formation of a dense and continuous TGO layer consisting mainly of α-Al_2O_3, trace amounts of chromium (Cr_2O_3), and a small amount of spinel (AB_2O_4) and FCC and BCC structures, having an average thickness of 5 μm ± 0.50 μm, as shown in Fig. 3d. In previous studies, Butler et al. examined the oxidation behavior at 1050°C of $Al_{20}Co_{25}Cr_{25}Ni_{25}Si_5$ and $Al_{15}Cr_{10}Co_{35-}Ni_{35}Si_5$ HEAs. They displayed the development of a continuous Al_2O_3 layer and a minor volume fraction of Cr_2O_3.[37] Our results are following previous work by Butler et al. and shows the slow formation of the exclusive oxide scale on the surface of the bond coats.[37]

XRD Analysis for Phase Identification

XRD investigation was carried out for the phase identification and crystal structure of the present compounds of the high-entropy coatings, and was carried out at all stages and in all states, i.e., in as-sprayed, as-annealed states, as well as after the ITO testing of the respective bond coats. XRD analysis of the APS coatings in the as-coated conditions revealed BCC and FCC as the major phases, or we can say that a multitude of BCC and FCC phases were detected.[30] It can be seen that the as-sprayed coatings mostly consisted of pure metals with BCC and FCC crystal structures, except for minor quantities of Fe-Cr, FeO, and spinel formation, which can be elucidated from the XRD peaks.[30] In tallying, due to the high plasma jet temperature, in-flight oxidation ascends in the APS process, and peaks of mixed spinel oxides, marked ♥, AB_2O_4 (A = Ni/Co/Fe, B = Al/Cr) were also detected.[30,38]

All the diffraction peaks correspond well with previously published work,[39] as we do not have known accepted patterns or reference cards for the concerned alloy and alloy system. The crystal structure belongs to the cubic system. Major peaks demonstrating the BCC and FCC are found to be present.[30] Some of the diffraction peaks are marginally shifted in contrast to already published work on this alloy system because of the[30] low-energy ball-milling of our elemental powders, which do not make HEA at the ball-milling stage, and also the
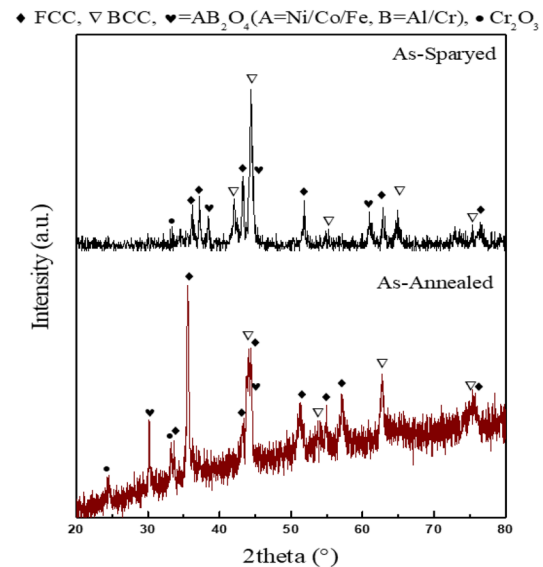

Fig. 4. XRD analysis of the coatings in as-coated and as-annealed conditions.

variance in the atomic radii of Ni, Fe, Cr, Al, and Co. The XRD patterns of the as-coated and annealed coatings are shown in Fig. 4.

High-entropy APS coatings were successively annealed at 900°C for 4 h in a tube furnace at SCME, having an inert atmosphere containing Ar, and XRD analysis was carried out after the vacuum annealing treatment. After the annealing, the content of Cr-O increased in the coatings, while the presence of pure metal content was minimized, which was similarly found by Lin et al.[30,39] Due to heat treatment at 900°C for 4 h, elemental diffusion took place to a larger extent, which considerably improved the entropy of our system and halted the formation of intermetallic compounds which are the ordered phases. The increase in the entropy of the system lowered the free energy of the alloy system, thus making stable solid solutions,[30,35] and revealing BCC and FCC as the major phases present in the coating microstructure. Some peaks of mixed spinel oxides (marked ♥), AB_2O_4 (A = Ni/Co/Fe, B = Al/Cr) were also discovered, due to the oxidation of the in-flight particles because of the high temperature of the plasma found earlier in the as-sprayed condition. The crystal structure belongs to the cubic system. Major peaks representing the BCC and FCC were found to be present. Some of the diffraction peaks are slightly shifted from their positions on the XRD diffractograms of the as-coated states.[30] As the intensity of the peak at the 2θ value of 37.16 increased, the peak for spinel at the 2θ of 38 changed to FCC, and the peak at the 2θ of 41 also divided into three smaller peaks for BCC, FCC, and spinel. The peak of the BCC structure present at a 2θ value of 42° disappeared. This phenomenon is since the annealing treatment of our plasma-sprayed coatings in the inert atmosphere,
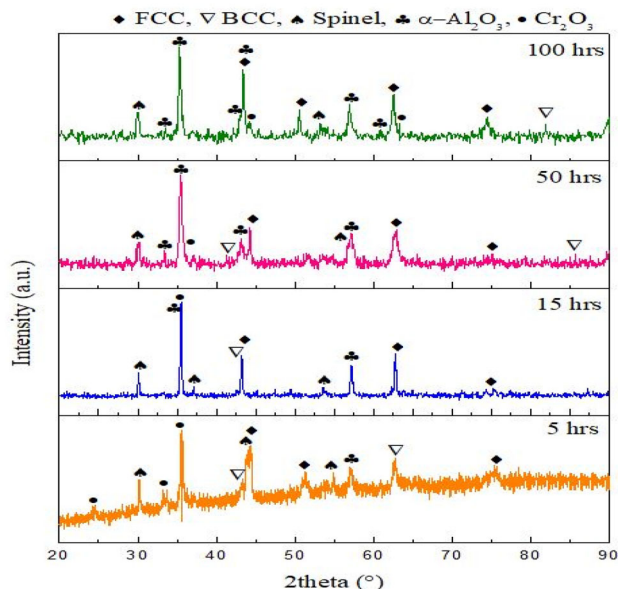
Development of Cost-Effective Microstructure and Isothermal Oxidation-Resistant Bond Coats
on Inconel 718 by Atmospheric Plasma-Sprayed NiCoCrAlFe High-Entropy Alloy

245

Fig. 5. XRD analysis after oxidation testing for different time.

Table III. Micro-hardness values of substrate and coatings in different conditions

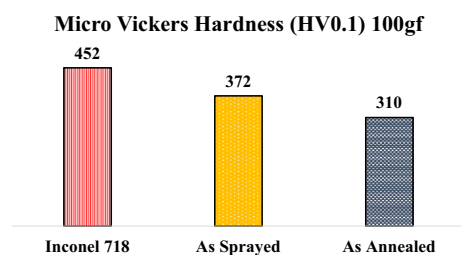|		Micro-Vickers's hardness		
Load	Dwell time	Inconel 718	Coated	Annealed
100 g	15 s	452	372	310

Fig. 6. Micro-Vickers hardness of Inconel 718, APS bond coat, and annealed bond coat.
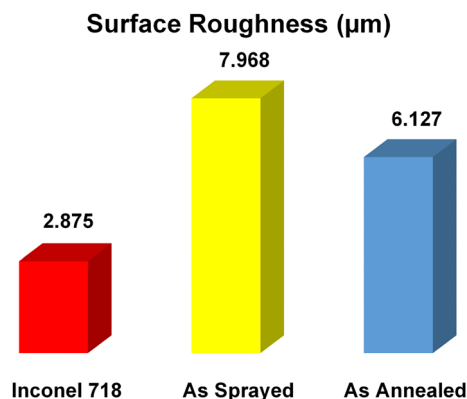

Fig. 7. Surface roughness (μm).

leading to HEA formation by slow diffusion of atoms with each other, which was not achieved completely at the earlier low-energy ball-milling stage.

ITO testing of the annealed bond coats was performed in the Nabetherm muffle furnace at a temperature of 1000°C for 5 h, 15 h, 50 h, and 100 h. It was found that, for the 5-h oxidation tests, the XRD peaks showed no significant changes from its annealed structure, but some phases were changed a little to the HEA alloy phase after 15 h of oxidation testing. The major phases are FCC and BCC. Some traces of spinel and chromia at different points were observed by looking at the position of the peak corresponding to the different phases present. While looking at the XRD pattern for the oxidation testing for 50 h, the peak positions revealed the formation of an uneven TGO layer consisting of α-Al_2O_3, chromia (Cr_2O_3), FCC, and BCC, along with a small amount of spinel (AB_2O_4) formation, as shown in Fig. 5. The ITO testing for 100 h shows that the TGO which has been grown in the bond coat is continuous and dense, consisting mainly of α-Al_2O_3 and formed along with NiO, AlN_3, FCC, and Cr_2O_3. The thickness of the TGO increased with the increased oxidation time, and was 5 μm $\pm$ 0.5 μm for 100 h exposure. The protective layer of the Al_2O_3 prevents augmented oxidation and improves the oxidation resistance of the prepared HEA bond coats.

Micro-Vickers Hardness

Hardness is the ability of a material to resist localized plastic deformation.[40] Four tests were performed for each sample and the readings were recorded as the average. Proper grinding and polishing are required for sample preparation to carry out hardness testing of samples.[41,42] While performing the heat treatment of our samples at the elevated temperature of 900°C, we had a greater extent of elemental diffusion. As there was a somewhat random distribution of different mixed elements, oxide stringers were also formed in the microstructure, which can be deemed as a possible reason for the high hardness value, while, in the case of the annealed coatings, it is evident that a maximum HEA fraction is formed, which decreases the free energy of the coatings. We can conclude that a solid solution was formed after annealing, which increased the extent of lattice distortion and inhibited dislocation motions. Alloy fractions have lower hardness values, which are achieved in the case of annealed coatings as compared to the as-sprayed coatings. Micro-Vicker's hardness values of the bare Inconel 718 substrate, the APS bond coat, and the annealed bond coats are set out in Table III, and also illustrated graphically in Fig. 6.

Roughness Testing

The surface was cleaned for the examination so that we could obtain true values for the observed roughness values of our different samples. Four readings were carried out and then an average was taken for each coated sample. After observing the roughness values of the samples in the as-coated condition and after subsequent heat treatment (annealing), we deduced that, upon plasma spraying, the particles were found in molten and semi-molten forms which adhered to the substrate in the form of a coating, so that the coating had a higher roughness value than the annealed coating. As soon as we annealed the coatings, the roughness began to reduce as the temperature applied in annealing favored HEA formation, and, due to the diffusion of the particles, the surface roughness was reduced as compared to their respective coatings. The results are summarized in graphical form in Fig. 7.

CONCLUSION

It is concluded that:

1. The bond coats resulting from APS comprise various scattered phases, including BCC and FCC, in the lamellar structure.
2. The lamellar pores in the bond coats closed upon controlled atmosphere heat treatment (annealing), and, consequently, the NiCoCrAlFe HEA was formed due to thermal diffusion.
3. The fabricated bond coats exhibit excellent oxidation resistance, which is an attribute of the progression of the TGO layer enriched in α-Al_2O_3. Even upon exposure to high temperatures for 100 h, the TGO thickness was 5 μm $\pm$ 0.5 μm and was continuous and dense.
4. Owing to slow oxide scale (TGO) formation, the respective NiCoCrAlFe bond coats have the potential to be used for high-temperature applications.

CONFLICT OF INTEREST

The authors declare no conflict of interest.

REFERENCES

1. X. Jun, C.-M. Cao, G. Ping, and L.-M. Peng, *Trans. Nonferr. Metal Soc.* 30, 746. https://doi.org/10.1016/S1003-6326(20)65250-5 (2020).
2. J.W. Yeh, S.K. Chen, S.J. Lin, J.Y. Gan, T.S. Chin, T.T. Shun, C.H. Tsau, and S.Y. Chang, *Adv. Eng. Mater.* 6, 299. https://doi.org/10.1002/adem.200300567 (2004).
3. B. Cantor, I. Chang, P. Knight, and A. Vincent, *Mater. Sci. Eng. A* 375, 213. https://doi.org/10.1016/j.msea.2003.10.257 (2004).
4. J. Yu, X. Lin, J. Wang, J. Chen, and W. Huang, *Appl. Surf. Sci.* 255, 9032. https://doi.org/10.1016/j.apsusc.2009.06.087 (2009).
5. Z. Li, S. Zhao, R.O. Ritchie, and M.A. Meyers, *Prog. Mater. Sci* 102, 296. https://doi.org/10.1016/j.pmatsci.2018.12.003 (2019).
6. H. Diao, X. Xie, F. Sun, K.A. Dahmen and P.K. Liaw, HEA 181–236 (2016). doi:https://doi.org/10.1007/978-3-319-27013-5_6.
7. G.-H. Meng, B.-Y. Zhang, H. Liu, G.-J. Yang, T. Xu, C.-X. Li, and C.-J. Li, *Surf. Coat. Technol.* 347, 54. https://doi.org/10.1016/j.surfcoat.2018.04.068 (2018).
8. Y. Zhang, T.T. Zuo, Z. Tang, M.C. Gao, K.A. Dahmen, P.K. Liaw, and Z.P. Lu, *Prog. Mater. Sci* 61, 1. https://doi.org/10.1016/j.pmatsci.2013.10.001 (2014).
9. X.-W. Qiu, Y.-P. Zhang, L. He, and C.-G. Liu, *J. Alloys Compd.* 549, 195. https://doi.org/10.1016/j.jallcom.2012.09.091 (2013).
10. Z. Cui, Z. Qin, P. Dong, Y. Mi, D. Gong, and W. Li, *Mater. Lett.* 259, 126769. https://doi.org/10.1016/j.matlet.2019.126769 (2020).
11. A. Erdogan, and K.M. Doleker, *Trans Nonferr Metal Soc* 31, 2428. https://doi.org/10.1016/S1003-6326(21)65664-9 (2021).
12. M. Kandeva, E. Zadorozhnaya, Z. Kalitchin, and P. Svoboda, *J. Balk. Tribol. Assoc.* 24, 411. (2018).
13. T. Sidhu, S. Prakash, and R. Agrawal, *Acta Mater.* 54, 773. https://doi.org/10.1016/j.actamat.2005.10.009 (2006).
14. M. Srivastava, M. Jadhav, R. Chakradhar, M. Muniprakash, and S. Singh, *Surf. Coat. Technol.* 378, 124950. https://doi.org/10.1016/j.surfcoat.2019.124950 (2019).
15. C.Y. Yap, C.K. Chua, Z.L. Dong, Z.H. Liu, D.Q. Zhang, L.E. Loh, and S.L. Sing, *Appl. Phys. Rev.* 2, 041101. https://doi.org/10.1063/1.4935926 (2015).
16. J. Lapin, T. Pelachová, and M. Dománková, *Intermetallics (Barking)* 95, 24. https://doi.org/10.1016/j.intermet.2018.01.013 (2018).
17. Y.-J. Xie, and M.-C. Wang, *Surf. Coat. Technol.* 201, 3564. https://doi.org/10.1016/j.surfcoat.2006.08.107 (2006).
18. L. Pawlowski, *The science and engineering of thermal spray coatings* (Wiley, London, 2008).
19. W. Ruijun, Q. Yiyu, and L. Jun, *Appl. Surf. Sci.* 240, 42. https://doi.org/10.1016/j.apsusc.2004.05.299 (2005).
20. G. Kirik, O. Gaponova, V. Tarelnyk, O. Myslyvchenko, and B. Antoszewski, *Powder Metall. Met. Ceram.* 56, 688. https://doi.org/10.1007/s11106-018-9944-6 (2018).
21. C. Wu, S. Zhang, C. Zhang, J. Chen, and S. Dong, *Opt Laser Technol.* 94, 68. https://doi.org/10.1016/j.optlastec.2017.03.023 (2017).
22. G. Jin, Z. Cai, Y. Guan, X. Cui, Z. Liu, Y. Li, and M. Dong, *Appl. Surf. Sci.* 445, 113. https://doi.org/10.1016/j.apsusc.2018.03.135 (2018).
23. B. Gill, and R. Tucker, *Mater. Sci.* 2, 207. https://doi.org/10.1179/mst.1986.2.3.207 (1986).
24. P. Fauchais, M. Vardelle, A. Vardelle, and L. Bianchi, *Ceram. Int.* 22, 295. https://doi.org/10.1016/0272-8842(95)00106-9 (1996).
25. M. Löbel, T. Lindner, C. Kohrt and T. Lampke, In *IOP Conference Series: Mater. Sci. Eng.* (IOP Publishing: 2017), p. 012015. https://doi.org/10.1088/1757-899X/181/1/012015.
26. J.-K. Xiao, H. Tan, Y.-Q. Wu, J. Chen, and C. Zhang, *Surf. Coat. Technol.* 385, 125430. https://doi.org/10.1016/j.surfcoat.2020.125430 (2020).
27. N. Tan, Z.-G. Xing, X.-L. Wang, H.-D. Wang, G. Jin, and B.-S.J. Xu, *J. Mater. Res.* 32, 1682. https://doi.org/10.1557/jmr.2017.164 (2017).
28. C. Chen, N. Liu, J. Zhang, J. Cao, L. Wang, and H. Xiang, *J Mater Sci Technol* 35, 1883. https://doi.org/10.1080/02670836.2019.1652785 (2019).
29. N.K. Adomako, J.H. Kim, and Y.T. Hyun, *J. Therm. Anal. Calorim.* 133, 13. https://doi.org/10.1007/s10973-018-6963-y (2018).
30. K. Mehmood, M.A. Umer, A.U. Munawar, M. Imran, M. Shahid, M. Ilyas, R. Firdous, H. Kousar, and M. Usman, *Materials* 15, 1486. https://doi.org/10.3390/ma15041486 (2022).
31. A.S. Ang, C.C. Berndt, M.L. Sesso, A. Anupam, P.S.R.S. Kottada and B. Murty, Comparison of Plasma Sprayed High Entropy Alloys with Conventional Bond Coat Materials. Paper presented at International Thermal Spray Confer-

Development of Cost-Effective Microstructure and Isothermal Oxidation-Resistant Bond Coats
on Inconel 718 by Atmospheric Plasma-Sprayed NiCoCrAlFe High-Entropy Alloy
247

ence, Long Beach, California, USA, 11–14 May 2015. https://doi.org/10.31399/asm.cp.itsc2015p0027.

32. M. Kumar, M. Das, J.D. Majumdar, and I. Manna, *Surf. Coat. Technol.* 402, 126345. https://doi.org/10.1016/j.surfcoat.2020.126345 (2020).

33. K.M. Döleker, A. Erdogan, T. Yener, A.C. Karaoglanlı, O. Uzun, M.S. Gök, and S. Zeytin, *Surf. Coat. Technol.* 412, 127069. https://doi.org/10.1016/j.surfcoat.2021.127069 (2021).

34. A.S.M. Ang, C.C. Berndt, M.L. Sesso, A. Anupam, S. Praveen, R.S. Kottada, and B. Murty, *Metall Mater Trans A Phys Metall Mater Sci.* 46, 791. https://doi.org/10.1007/s11661-014-2644-z (2015).

35. A. Meghwal, A. Anupam, V. Luzin, C. Schulz, C. Hall, B. Murty, R.S. Kottada, C.C. Berndt, and A.S.M.J. Ang, *J. Alloys Compd.* 854, 157140. https://doi.org/10.1016/j.jallcom.2020.157140 (2021).

36. S.W. Rukhande, and W.S. Rathod, *Ceram. Int.* 46, 18498. https://doi.org/10.1016/j.ceramint.2020.04.155 (2020).

37. T. Butler, J. Alfano, R. Martens, and M. Weaver, *JOM* 67, 246. https://doi.org/10.1007/s11837-014-1185-7 (2015).

38. M. Imran, Z. Saeed, M. Pervaiz, K. Mehmood, R. Ejaz, U. Younas, H.A. Nadeem, S. Hussain, and B. Spectroscopy, *Spectrochim. Acta A Mol. Biomol. Spectrosc.* 255, 119644. https://doi.org/10.1016/j.saa.2021.119644 (2021).

39. D.-Y. Lin, N.-N. Zhang, B. He, B.-Q. Jin, Y. Zhang, D.-Y. Li, and F.-Y. Dong, *J. Iron Steel Res. Int.* 24, 1199. https://doi.org/10.1016/S1006-706X(18)30018-9 (2017).

40. H. Grewal, H. Singh, and A. Agrawal, *Surf. Coat. Technol.* 216, 78. https://doi.org/10.1016/j.surfcoat.2012.11.029 (2013).

41. L. Baiamonte, C. Bartuli, F. Marra, A. Gisario, and G. Pulci, *Coatings* 9, 347. https://doi.org/10.3390/coatings9060347 (2019).

42. N. Arshad, M. Imran, M. Akram, and F. Altaf, *Port. Electrochimica Acta* 40(3), 193. https://doi.org/10.4152/pea.2022400304 (2022).